Engineering Structures 288 (2023) 116224

Contents lists available at ScienceDirect

Engineering Structures

journal homepage: www.elsevier.com/locate/engstruct

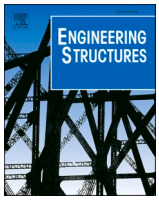

Uncertainty analysis of inelastic response of high-rise buildings to wind using a reduced-order building model

Jinghui Huang, Xinzhong Chen *

National Wind Institute, Department of Civil, Environmental and Construction Engineering, Texas Tech University, Lubbock, TX 79409-1023, United States

ARTICLE INFO

Keywords:
High-rise building
Inelastic response
Reduced-order building model
Uncertainty analysis
Extreme value distribution
Time-varying mean alongwind displacement

ABSTRACT

The influence of various uncertainties on wind-induced inelastic building response is quantified through response time history simulation of a reduced-order building model of a 60-story steel building as an example. The reduced-order building model and its uncertainties are established through modal push-over analysis of a high-fidelity nonlinear finite element building model with distributed plasticity. The basic uncertain parameters are modal mass, stiffness, damping ratio and yielding displacement as well as loading power spectra. The results demonstrated that the uncertainty of response standard deviation (STD) is mainly contributed by uncertainty of modal damping ratio for elastic response, while it is further contributed by the uncertainty of the yielding displacement for inelastic response. The uncertainty of inelastic response with a higher level of yielding is less than that of elastic response. The uncertainty in extreme response is also determined in terms of the influences of randomness, sampling uncertainty and parameter uncertainty. The results showed that the influence of randomness can be accurately estimated using the crossing rate theory with consideration of non-Gaussian response character. The influence of sampling and parameter uncertainties on extreme response reduces with increasing level of yielding. The uncertainty in the time-varying mean alongwind displacement is also quantified, which is very sensitive to building yielding displacement.

1. Introduction

Current design of tall buildings for wind is based on linear framework in which building behaves in linear elastic even under strong wind with a very low exceeding probability. The linear design approach may limit the use of more innovative tall building systems with improved performance and economy. The ASCE has recently published pre-standard for performance-based wind design (PBWD) of buildings [2], which explicitly permits nonlinear dynamic analysis allowing limited inelasticity in the Main Wind Force Resisting System (MWFRS) elements.

There are numbers of research efforts addressing inelastic performance of tall buildings to wind [49,28,27,21,23,3,31,38,32,33,22,41,29]. The building model used for inelastic response analysis ranges from a single degree of freedom model, two-dimensional (2D) finite element (FE) model to 3D FE model with various degrees of nonlinearities. The nonlinear relationship between joint forces and displacements of each building member can be considered using different models, such as plastic hinge, nonlinear spring hinge, finite length hinge zone, fiber section, and finite element models [39]. The FE model provides detailed information of building responses but is computationally demanding.

Studies have shown that the inelastic tall building response to wind is also dominated by fundamental modes similar to elastic response [29]. Several studies have focused on simplified estimations of uncoupled alongwind and crosswind inelastic responses of tall buildings [40,51,19] and [20]. Feng and Chen [19] and [20] presented comprehensive studies on both inelastic alongwind and crosswind responses by considering the fundamental modes with bilinear restoring force character through time history analysis and statistical linearization approaches. Huang and Chen [30] carried out inelastic building response analysis using a reduced-order building model, in which the building response is represented by fundamental modal displacements, and the hysteretic relations between the generalized restoring forces and displacements are determined by static modal push-over analysis (MPA) using a nonlinear FE building model. [29] and [30] addressed the biaxial interaction of alongwind and crosswind responses under simultaneous actions of both alongwind and crosswind loadings.

One of the distinct characters of inelastic building response to wind from those to seismic loading is the existence of time-varying mean

* Corresponding author.
E-mail addresses: jinghui.huang@ttu.edu (J. Huang), xinzhong.chen@ttu.edu (X. Chen).

https://doi.org/10.1016/j.engstruct.2023.116224
Received 27 March 2022; Received in revised form 13 March 2023; Accepted 23 April 2023

displacement due to the action of mean (static) alongwind load. The yielding causes building to drift in alongwind direction, and the building vibrates about the new equilibrium until it gets shifted again by another yielding. The drift leads to low-frequency displacement component. The development of time-varying mean displacement is affected by dynamic response, while its steady-state is determined by the mean load and post-yielding building stiffness. The dynamic response around the time-varying mean displacement is not influenced by the time-varying mean response, thus can be computed under dynamic wind loading without mean load component [44,20,30].

The reliability-based performance evaluation of wind-excited tall buildings requires consideration of various uncertainties in wind load and structural model parameters. Assessment of reliability or failure probability of buildings to wind can employ Monte Carlo simulation (MCS) procedure. Use of static response analysis in the MCS procedure with a model of equivalent static wind load (e.g., [18,17,16,24,4]) can greatly reduce the computational cost but cannot fully capture the uncertainties in dynamic wind loads and load effects. Spence and Kareem [47] presented an approach for probabilistic performance-based assessment of large-scale uncertain linear structures. Tabbuso et al. [48] proposed a method for evaluating elasto-plastic reliability of uncertain wind-excited structures using Subset Monte Carlo simulation of alongwind response. Chuang and Spence [8–10] investigated collapse probability and reliability assessment of tall buildings based on dynamic shakedown theory. Ouyang and Spence [41] carried out a probabilistic assessment of structural and envelop damage of a 45-story steel high-rise building through nonlinear dynamic history analysis using a fiber section-based nonlinear FE model. Zheng et al. [54] presented a reliability-based approach for high-rise buildings under the combined effects of earthquakes and strong winds. The development of analysis approaches for addressing the effect of various uncertainty parameters on dynamic responses of linear structural systems has been discussed in Lutes and Sarkani [35] and among others. Research efforts continue especially for nonlinear structural systems.

The conditional probability assessment procedures on a given wind speed and direction are more effective for assessing reliability of wind-excited buildings, thus is more practical for adoption in design codes and standards [11] and [12]; [25] and [26]; [7], [5], [53]; [2]. The probabilistic limit state responses under given wind speed and direction are determined from Monte Carlo simulation and other approaches. The fragility functions are then quantified by further accounting for the probability distributions of capacities. The failure probability is then evaluated by further integrating the joint probability distribution of wind speed and direction [53,34,50].

In this study, various uncertainties in inelastic response evaluation of wind-excited tall buildings are identified and quantified. The influences of these uncertainties on building top displacement and acceleration are quantified through Monte Carlo simulations of response time history using a reduced-order building model. The reduced-order building model was developed from MPA from a high-fidelity nonlinear FE building model with distributed plasticity. The uncertainties in hysteretic restoring force models are determined through Monte Carlo simulation of static push-over analysis with uncertain stress–strain relation of the structural materials, which capture the propagation of uncertainties from basic input uncertain parameters to the generalized restoring forces. The model parameters that have the most significant impact on the critical responses are identified. The probabilistic extreme displacement and acceleration considering randomness of wind loading and uncertainty of various model parameters and sampling uncertainty are characterized. The uncertainty in the time-varying mean alongwind displacement is also quantified. The total uncertainty in response is clearly characterized in terms of randomness, sampling uncertainty and parameter uncertainty. With the quantification of probabilistic demands, the fragility or system reliability can be further quantified by considering the uncertainties of capacities.

2. Inelastic building response analysis approach

A reduced-order building model in terms of fundamental building modal displacements can be developed using MPA procedure. By representing the heightwise building displacements in terms of fundamental modal displacements in two translational x and y directions, the coupled equations of modal displacements are described as [30]:

$$M_x\ddot{q}_x(t)+2M_x\zeta_x\omega_x\dot{q}_x(t)+F_{sx}\left(q_x,\dot{q}_x,q_y,\dot{q}_y\right)=Q_x(t) \tag{1a}$$

$$M_y\ddot{q}_y(t)+2M_y\zeta_y\omega_y\dot{q}_y(t)+F_{sy}\left(q_x,\dot{q}_x,q_y,\dot{q}_y\right)=Q_y(t) \tag{1b}$$

where $q_x(t)$ and $q_y(t)$ are generalized displacements; M_x, ω_x, ζ_x, $Q_x(t)$ and M_y, ω_y, ζ_y, $Q_y(t)$ are generalized mass, modal circular frequency, damping ratio, and generalized wind load in two directions; F_{sx} and F_{sy} are generalized restoring forces. When building response is within linear elastic range and also the centers of mass and stiffness coincide, i.e., building has no eccentricity, $F_{sx}\left(q_x,\dot{q}_x,q_y,\dot{q}_y\right)=K_xq_x=M_x\omega_x^2q_x$ and $F_{sy}\left(q_x,\dot{q}_x,q_y,\dot{q}_y\right)=K_yq_y=M_y\omega_y^2q_y$, , thus the equations of motion are uncoupled. When building behaves beyond linear elastic range, the generalized restoring forces are described in hysteretic relations with displacements and velocities. The equations of motion become coupled as the relationship between the restoring force and displacement in one direction is also affected by the response in another direction. The hysteretic generalized restoring forces can be quantified via static MPA procedure using static analysis of a nonlinear FE building model [29].

The generalized restoring forces F_{sx} and F_{sy} are expressed as the following biaxial hysteretic model [52]:

$$F_{sx}=\alpha_xK_xq_x+(1-\alpha_x)K_xz_x \tag{2a}$$

$$F_{sy}=\alpha_yK_yq_y+(1-\alpha_y)K_yz_y \tag{2b}$$

$$\dot{z}_x=A_x\dot{q}_x-z_xI \tag{3a}$$

$$\dot{z}_y=A_y\dot{q}_y-z_yI \tag{3b}$$

$$I=\left|\dot{q}_x\right|\left|z_x\right|^{n-1}\left[\beta_0+\gamma_0\mathrm{sgn}\left(\dot{q}_xz_x\right)\right]\Big/\Delta_x^n+\left|\dot{q}_y\right|\left|z_y\right|^{n-1}\left[\beta_0+\gamma_0\mathrm{sgn}\left(\dot{q}_yz_y\right)\right]\Big/\Delta_y^n \tag{3c}$$

where α_x and α_y are second (post-yielding) stiffness ratios; z_x and z_y are hysteretic displacements; sgn $(\cdot)$ is sign function; $A_x=A_y=1$ in general; Δ_x and Δ_y are yield displacements under uniaxial loads in x and y directions, respectively. The shape parameter n determines the smoothness of transition from pre-yielding to post-yielding region; $\beta_0+\gamma_0=1$, and often $\beta_0=\gamma_0=0.5$.

The equation of building motion is solved by using step-by-step integration method. The dynamic wind load time history sample is simulated from loading power spectra using spectral representation method and others [45,6]. The building response can also be calculated using statistical linearization approach which permits use of spectral analysis procedure (e.g., [30].)

Huang and Chen [29] and [30] have presented a comprehensive study of inelastic response of a 60-story steel building under biaxial alongwind and crosswind loadings using a nonlinear FE model with distributed plasticity and a reduced-order model. The results showed that the reduced-order model can effectively and accurately predict the response statistics including response STD, peak factors, and kurtosis at different wind speeds. On the other hand, the time-varying mean response is overestimated by the reduced-order building model.

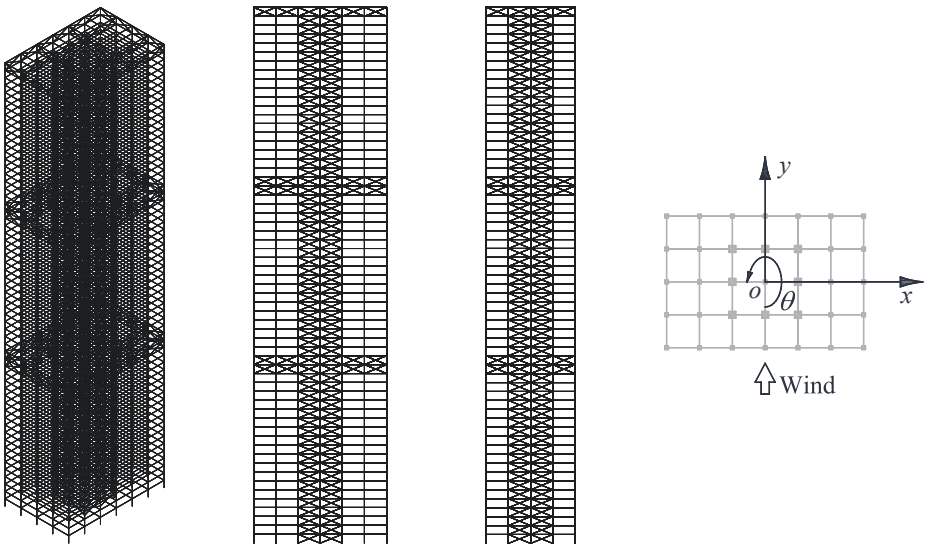

Fig. 1. FE model of the building frame.

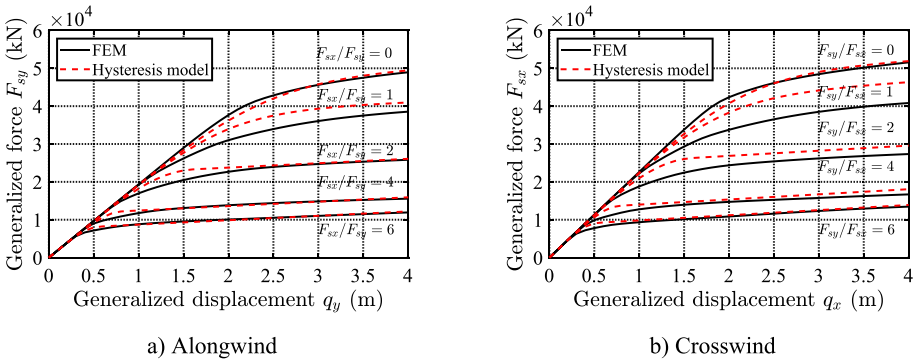

Fig. 2. Generalized restoring force and displacement relations.

3. Building model with uncertain parameters

3.1. A tall building model

A 60-story high-rise steel structure with 182.88 m height, 45.72 m width, and 30.48 m depth is considered (Fig. 1). The building is a replica of the CAARC building with distributed non-linear stiffness in members and it has an outrigger system at three elevations, i.e., 20th and 21st, 40th and 41st, and 60th floors, and a core bracing system to resist the lateral load. A 3D nonlinear FE model is constructed in the OpenSees environment [36]. The building frame is consisted of 2,100 columns, 3,480 beams, and 2,560 diagonal bracings, including a total of 16 types of member sections. All members are represented in fiber section-based nonlinear model [39]and each element has five fiber sections [46]. More than 300 fibers over each column and bracing cross-sectional area, and more than 150 fibers over each beam cross-sectional area are used. The nonlinearity of the steel material is described by a bilinear model with a yield stress of 345 MPa and a post-yielding stiffness ratio 0.01. The two fundamental frequencies in two translational directions, i.e., x and y directions, are $f_x = 0.173$ Hz and $f_y = 0.164$ Hz. The modal damping ratios are assumed to be $\zeta_x = \zeta_y = 1\%$. More detailed information about the FE model can be found in Park and Yeo [42] and Huang and Chen [29]. The torsional wind load and response are quite low thus are not considered in this study. The wind is along y direction.

Fig. 2 shows the generalized restoring force–displacement (building top displacement) relations for different values of F_{sy}/F_{sx} determined by MPA. The cases $F_{sy}/F_{sx} = 0$ and $F_{sx}/F_{sy} = 0$ correspond to uniaxial loads in x and y directions, respectively. It is evident that the yield displacement in one direction reduces with the increase of load in another direction. The uniaxial hysteretic models are fitted for both directions with $n = 4$, $\alpha_x = \alpha_y = 0.06$, $\Delta_x = 2.2$ m, and $\Delta_y = 2.5$ m. The biaxial model is accordingly determined using the model parameters under uniaxial loads. It is seen that the biaxial model can well describe the hysteretic relation of the generalized forces and displacements.

3.2. Wind loading model

The alongwind static wind force at i-th story is determined as:

$$\overline{P}_i = 0.5\rho U_H^2 \overline{C}_D B H_0 \left(\frac{z_i}{H}\right)^{2\alpha_s} \tag{4}$$

where ρ is the air density, 1.22kg/m^3; U_H is the mean wind speed at the building top averaged in 10 min; B is the building width; H_0 is the story height and $H_0 = 3.048$m; H is the building height; z_i is the height of i-th floor; $\overline{C}_D$ is the constant drag force coefficient along the building height and is determined from the static coefficient of base bending moment $\overline{C}_M$ as $\overline{C}_D = 2\overline{C}_M(\alpha_s + 1)$; $\alpha_s = 0.2$ is the power law exponent of the wind speed profile for the suburban terrain.

The fluctuating components of alongwind story forces are modeled in terms of power spectral model. The cross power spectral density

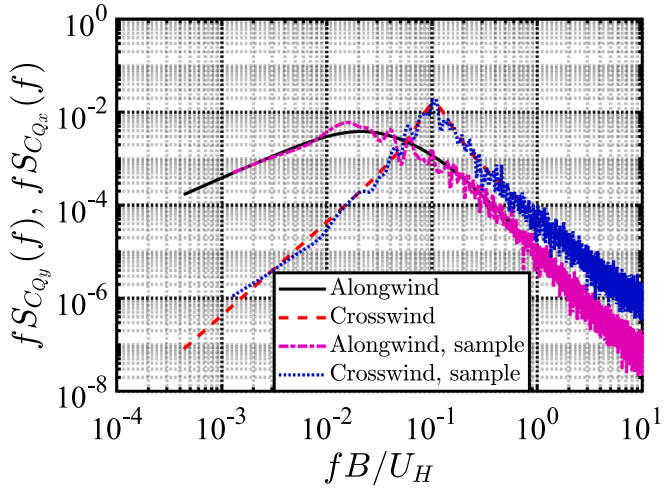

Fig. 3. Power spectra of generalized force coefficients.

Table 1
Statistics of basic random variables.

Variables	$\epsilon_{\sigma_{yield}}$	ϵ_E	ϵ_b	ϵ_K	ϵ_Δ	ϵ_M	ϵ_ζ	ϵ_{C_M}
Mean	1	1	1	1	1	1	1	1
CV	0.05	0.05	0.05	0.05	0.08	0.05	0.50	0.30

(CPSD) function of the i-th and j-th story forces is given as [6]:

$$S_{P_iP_j}(f) = S_{P_0}(f)\left(\frac{z_i}{H}\right)^{\alpha_s}\left(\frac{z_j}{H}\right)^{\alpha_s}\exp\left(-\frac{k_y fH}{U_H}\frac{|z_i - z_j|}{H}\right) \tag{5}$$

$$S_{P_0}(f) = \left(\frac{1}{2}\rho U_H^2 BH_0\right)^2 S_{C_M}(f)/|J_z(f)|^2 \tag{6}$$

$$|J_z(f)|^2 = \left(\frac{H_0}{H}\right)^2\sum_{i=1}^{N}\sum_{j=1}^{N}\left(\frac{z_i}{H}\right)^{\alpha_s+1}\left(\frac{z_j}{H}\right)^{\alpha_s+1}\exp\left(-\frac{k_z fH}{U_H}\frac{|z_i - z_j|}{H}\right) \tag{7}$$

where $S_{C_M}(f)$ is the power spectrum of the base bending moment coefficient $C_M(t)$; $k_z = 7$ is the decay factor for the alongwind load; N is the number of stories and $N = 60$. Same CPSD model is also used for crosswind story forces, but different spectrum $S_{C_M}(f)$ and decay factor $k_y = 5$ are adopted.

The power spectra of alongwind and crosswind base bending moment coefficients are given according to the AIJ recommendations [1;15]. The STD of alongwind $C_M(t)$ is $\sigma_{C_M} = 0.11$. For the crosswind $C_M(t)$, $\sigma_{C_M} = 0.1175$; the bandwidth parameter of the spectrum takes $\beta_1 = 0.28$; parameter $\kappa_1 = 0.85$; and the Strouhal number $S_t = 0.09$. The power spectra of generalized forces are calculated from the spectral model of the story forces. The alongwind and crosswind loadings are assumed to be independent.

Fig. 3 displays the power spectra of the generalized force coefficients in alongwind and crosswind directions, i.e., $C_{Q_y}(t) = Q_y(t)/(0.5\rho U_H^2 BH)$ and $C_{Q_x}(t) = Q_x(t)/(0.5\rho U_H^2 BH)$, which are very close to the power spectra of the base bending moment coefficients. The power spectrum of alongwind loading has higher low-frequency energy, while the power spectrum of crosswind loading exhibits a peak at the lock-in reduced frequency, $fB/U_H = S_t = 0.09$.

3.3. Uncertain parameters

It is assumed that the building mode shapes do not have uncertainty. The generalized mass are given as $M_x = M_{x0}\epsilon_M$ and $M_y = M_{y0}\epsilon_M$, and the modal damping ratios are $\zeta_x = \zeta_{x0}\epsilon_\zeta$ and $\zeta_y = \zeta_{y0}\epsilon_\zeta$, where M_{x0} and M_{y0}, ζ_{x0} and ζ_{y0} are the nominal (design) values; and ϵ_M and ϵ_ζ are random variables assumed to follow lognormal distributions with unit mean and coefficient of variation (CV) of 0.05 and 0.50, respectively (Table 1). The lognormal distribution is convenient and has been widely used for non-negative uncertainty parameters (e.g., [4;35;37]). It should be mentioned that assumed distribution models of important random variables can have limited influence on the predicted uncertainty of structural response when their CVs are large [35;37].

The uncertainties in the relations of generalized forces and displacements are determined from Monte Carlo simulation using static MPA with the FE model. The steel material parameters in terms of yield stress, Young's modulus and strain hardening ratio, σ_{yield}, E and b, are basic random variables, i.e., $\sigma_{yield} = \sigma_{yield0}\epsilon_{\sigma_{yield}}$, $E = E_0\epsilon_E$, and $b = b_0\epsilon_b$, where σ_{yield0}, E_0 and b_0 are nominal values; and $\epsilon_{\sigma_{yield}}$, ϵ_E and ϵ_b are random variables assumed to follow lognormal distributions with unit means and CVs of 0.05 (Table 1). All building members use same material properties, which will lead to a greater uncertainty in the generalized forces as compared to the case of using different material properties. Fig. 4 shows 50 samples of generalized force and displacement relations and the corresponding fitted hysteresis model under uniaxial loads. The curve fitting results of hysteretic model indicate that the model parameters α_x, α_y, n_x, and n_y remain almost unchanged; K_x and K_y, Δ_x and Δ_y are fully correlated, respectively. The correlation coefficient between K_x and Δ_x is −0.68. These uncertainty parameters can be modeled as $K_x = K_{x0}\epsilon_K$; $K_y = K_{y0}\epsilon_K$; $\Delta_x = \Delta_{x0}\epsilon_\Delta$ and $\Delta_y = \Delta_{y0}\epsilon_\Delta$, where K_{x0}, K_{y0}, Δ_{x0} and Δ_{y0} are nominal values; ϵ_K and ϵ_Δ are random variables following lognormal distributions with unit means and CVs of 0.05 and 0.08 according to the MPA simulation data. The correlation coefficient between ϵ_K and ϵ_Δ is −0.68, which is identical to that between K_x and Δ_x, as both are resulted from uncertainty of stress–strain relation of the steel material.

The samples of generalized restoring force–displacement relations are also generated for a given ratio F_{sy}/F_{sx}, which are fitted into a uniaxial hysteretic model, from which the yield displacements $\Delta_x(\theta)$ and

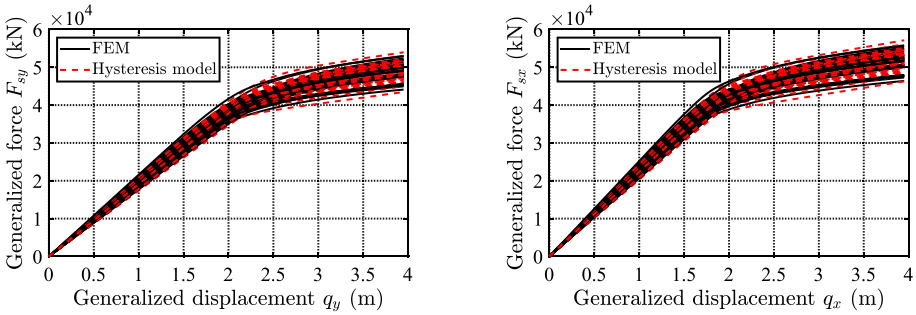

a) Alongwind MPA b) Crosswind MPA

Fig. 4. Variation of generalized restoring force and displacement relations.

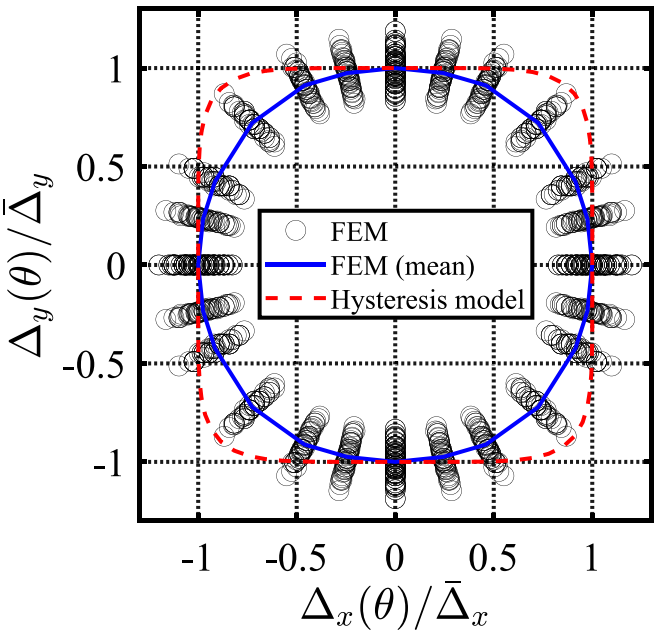

Fig. 5. Variation of yield surface.

$\Delta_y(\theta)$ are determined. Fig. 5 shows 50 samples of yielding displacement boundaries given in terms of $[\Delta_x(\theta)/\bar{\Delta}_x, \Delta_y(\theta)/\bar{\Delta}_y]$, where $\bar{\Delta}_x = \Delta_{x0}$ and $\bar{\Delta}_y = \Delta_{y0}$. The yielding boundary calculated from the biaxial model using the design values of the model parameters is also presented which is close to a square. As illustrated in Huang and Chen [30], the difference of this yielding boundary can, to some extent, affect the time-varying mean alongwind displacement, but has little influence on the dynamic response around the mean response.

The uncertainty in dynamic loading spectra is also considered by treating $S_{C_M}(f)$ as a random quantity, i.e., $S_{C_M}(f) = S_{C_{M0}}(f)\epsilon_{C_M}$, where $S_{C_{M0}}(f)$ is nominal value; and ϵ_{C_M} is a random variable assumed to follow a lognormal distribution with unit mean and CV of 0.30. Larger CVs are assumed for structural damping ratio and loading spectrum according to the knowledge of their uncertainties. The condition of zero uncertainty in structural properties and dynamic loading spectra can be simply achieved by setting zero value of CVs of the random variables in Table 1.

4. Uncertainty analysis of building response

4.1. Response STDs

When building response is within linear elastic, the alongwind and crosswind responses are uncorrelated and can be computed separately. For instance, the variances of modal displacement and acceleration in terms of building top displacement and acceleration in alongwind direction or crosswind direction can be estimated as

$$\sigma^2 = \sigma_B^2 + \sigma_R^2 \approx \frac{\sigma_Q^2}{K^2} + \frac{\pi f_0 S_Q(f_0)}{4K^2\zeta} = \frac{\sigma_Q^2}{K^2} + \frac{S_Q(f_0)}{8M^{1/2}K^{3/2}\zeta} \tag{8}$$

$$\sigma_a^2 \approx (2\pi f_0)^4 \sigma_R^2 = \frac{S_Q(f_0)}{8M^{5/2}K^{-1/2}\zeta} \tag{9}$$

where σ^2, σ_B^2 and σ_R^2 are variances of total, background and resonant displacement components; $S_Q(f_0)$ is the PSD of the generalized force at the modal frequency f_0; σ_Q^2 is variance of generalized force $Q(t)$; M, K and ζ are generalized mass, stiffness and damping ratio; σ_a^2 is the variance of acceleration. The index x and y are omitted here for simplicity. The background component of crosswind displacement of tall buildings is negligibly small. The background component of alongwind displacement reduces with increasing wind speed and becomes negligible at higher wind speeds.

Consider the uncertainties of the variances of displacements and accelerations resulted from the uncertainty of structural and loading parameters. The estimated σ^2 is considered to be unbiased $E[\sigma^2] = \sigma_0^2$ and with the variance calculated as:

$$\mathrm{Var}(\sigma^2) = \mathrm{Var}(\sigma_B^2) + \mathrm{Var}(\sigma_R^2) \tag{10}$$

Accordingly, the CV of σ^2 is given by

$$\beta_{\sigma^2} = \sqrt{\beta_{\sigma_B^2}^2 \left(\frac{\sigma_{B0}^2}{\sigma_0^2}\right)^2 + \beta_{\sigma_R^2}^2 \left(\frac{\sigma_{R0}^2}{\sigma_0^2}\right)^2} \tag{11}$$

where β_{σ^2}, $\beta_{\sigma_B^2}$ and $\beta_{\sigma_R^2}$ are CVs of the total, background and resonant variances; σ_0^2, σ_{B0}^2 and σ_{R0}^2 are the nominal values of variances, estimated without the parameter uncertainty.

By using the logarithmic perturbation method e.g., [35], the CVs of estimated background and resonant displacement variances and the CV of acceleration variance are calculated as:

$$\beta_{\sigma_B^2} = \sqrt{\beta_{\sigma_Q^2}^2 + 4\beta_{\epsilon_K}^2} \tag{12}$$

$$\beta_{\sigma_R^2} = \sqrt{\beta_{S_Q}^2 + \left(\frac{1}{2}\right)^2 \beta_{\epsilon_M}^2 + \left(\frac{3}{2}\right)^2 \beta_{\epsilon_K}^2 + \beta_{\epsilon_\zeta}^2} \tag{13}$$

$$\beta_{\sigma_a^2} = \sqrt{\beta_{S_Q}^2 + \left(\frac{5}{2}\right)^2 \beta_{\epsilon_M}^2 + \left(\frac{1}{2}\right)^2 \beta_{\epsilon_K}^2 + \beta_{\epsilon_\zeta}^2} \tag{14}$$

where $\beta_{\sigma_Q^2}$ and β_{S_Q} are CVs of σ_Q^2 and $S_Q(f_0)$, which can be estimated as $\beta_{\sigma_Q^2} = \beta_{\epsilon_{C_M}}$ and

$$\beta_{S_Q} = \sqrt{\left(\frac{dS_Q'(f_0)}{df'}\right)^2 \beta_{f_0}^2 + \beta_{\epsilon_{C_M}}^2} = \sqrt{\left(\frac{dS_Q'(f_0)}{df'}\right)^2 \frac{1}{4}(\beta_{\epsilon_K}^2 + \beta_{\epsilon_M}^2) + \beta_{\epsilon_{C_M}}^2} \tag{15}$$

in which $dS_Q'(f_0)/df'$ is the derivative of normalized spectrum $S_Q(f)/S_{Q_0}(f_0)$ with respective to the normalized frequency $f' = f/f_0$; and β_{f_0} is CV of modal frequency. Clearly, the uncertainty of $S_Q(f_0)$ is contributed by the uncertainties of the spectral model and the modal frequencies. According to the power spectra used in this study, this derivative is approximately equal to -3 and $-11/3$, respectively, for alongwind and crosswind loadings. Considering the assigned CVs of the basic random variables, i.e., Table 1, the influence of the uncertainty of modal frequency is relatively small, thus $\beta_{S_Q} \approx \beta_{\epsilon_{C_M}}$.

Subsequently, the following values of CVs are estimated:

$$\begin{aligned}
\beta_{\sigma_B^2} &= \sqrt{0.3^2 + 4(0.05)^2} = 0.316 \\
\beta_{\sigma_R^2} &= \sqrt{0.3^2 + \left(\frac{1}{2}\right)^2 (0.05)^2 + \left(\frac{3}{2}\right)^2 (0.05)^2 + 0.5^2} = 0.588 \\
\beta_{\sigma_a^2} &= \sqrt{0.3^2 + \left(\frac{5}{2}\right)^2 (0.05)^2 + \left(\frac{1}{2}\right)^2 (0.05)^2 + 0.5^2} = 0.596
\end{aligned} \tag{16}$$

The CVs of the STDs of displacement and acceleration are approximately calculated as $\beta_{\sigma_B} = 0.5\beta_{\sigma_B^2} = 0.158$; $\beta_{\sigma_R} = 0.5\beta_{\sigma_R^2} = 0.294$; $\beta_{\sigma_a} = 0.5\beta_{\sigma_a^2} = 0.298$. When the uncertainty of the loading spectrum is not included, these CVs are 0.05, 0.252, 0.258, respectively. It is noted that the sensitivity coefficients of the basic random variables ϵ_{C_M}, ϵ_M, ϵ_K and ϵ_ζ with respect to the CV of resonant displacement STD are 0.5, 0.25, 0.75 and 0.5, respectively. The sensitivity coefficients to the CV of acceleration STD are 0.5, 1.25, 0.25 and 0.5, respectively. In this study, the structural damping ratio is assigned to have significantly large uncertainty, which dominates the uncertainty of displacement and

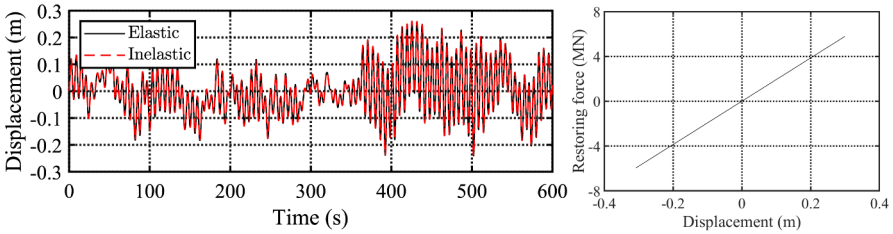

a) Alongwind displacement, $U_H = 40$ m/s

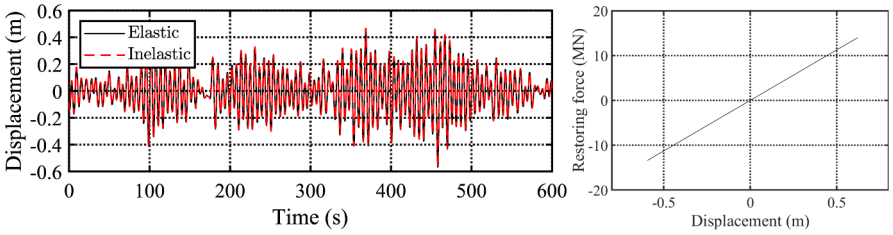

b) Crosswind displacement, $U_H = 40$ m/s

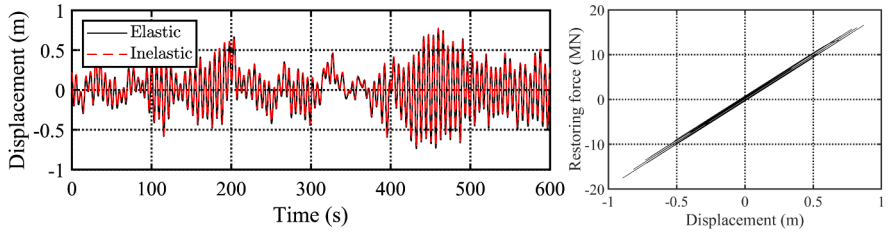

c) Alongwind displacement, $U_H = 60$ m/s

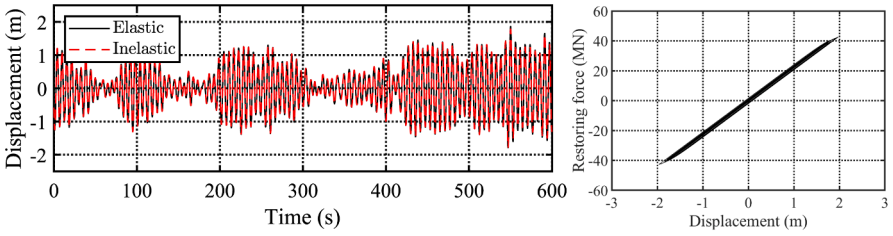

d) Crosswind displacement, $U_H = 60$ m/s

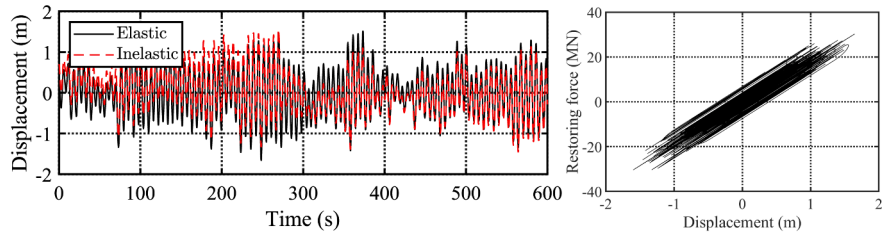

e) Alongwind displacement, $U_H = 80$ m/s

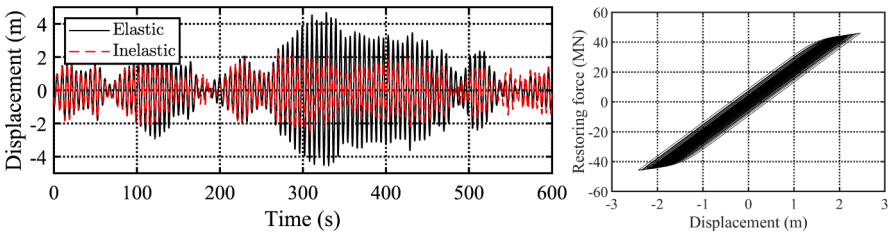

f) Crosswind displacement, $U_H = 80$ m/s

Fig. 6. Response time history samples and the relations of generalized restoring forces and displacements.

Table 2
Mean and CV of statistics of displacements with parameter uncertainty ($T = 10$mins).

Direction	U_H(m/s)	Response STD, σ		Crossing rate, ν_0		Kurtosis		Extreme, non-Gaussian		Mean extreme, non-Gaussian		Extreme sample	
		mean	CV	mean	CV	mean	CV	mean	CV	mean	CV	mean	CV
Alongwind	40	0.093	0.292	0.141	0.081	2.743	0.122	0.288	0.089	0.277	0.262	0.281	0.264
	60	0.271	0.286	0.149	0.058	2.779	0.123	0.854	0.091	0.818	0.261	0.828	0.257
	80	0.517	0.230	0.150	0.050	2.812	0.125	1.648	0.093	1.577	0.227	1.658	0.231
Crosswind	40	0.172	0.358	0.165	0.039	2.675	0.143	0.524	0.082	0.502	0.308	0.497	0.287
	60	0.641	0.240	0.170	0.033	2.532	0.129	1.856	0.073	1.820	0.202	1.742	0.190
	80	0.975	0.129	0.171	0.031	2.206	0.105	2.478	0.058	2.479	0.096	2.359	0.101

Table 3
Mean and CV of statistics of displacements with parameter uncertainty ($T = 60$mins).

Direction	U_H(m/s)	Response STD, σ		Crossing rate, ν_0		Kurtosis		Extreme, non-Gaussian		Mean extreme, non-Gaussian		Extreme sample	
		mean	CV	mean	CV	mean	CV	mean	CV	mean	CV	mean	CV
Alongwind	40	0.094	0.263	0.142	0.065	2.928	0.062	0.351	0.077	0.339	0.249	0.339	0.247
	60	0.280	0.239	0.151	0.045	2.986	0.094	1.079	0.081	1.003	0.230	1.030	0.254
	80	0.536	0.194	0.148	0.042	3.015	0.072	2.063	0.081	1.944	0.203	2.008	0.197
Crosswind	40	0.172	0.310	0.166	0.036	2.919	0.089	0.649	0.075	0.611	0.295	0.608	0.284
	60	0.656	0.191	0.170	0.032	2.628	0.088	2.183	0.058	2.156	0.139	1.991	0.128
	80	0.974	0.107	0.171	0.030	2.217	0.065	2.679	0.043	2.681	0.080	2.523	0.094

Table 4
Mean and CV of statistics of displacements without parameter uncertainty ($T = 10$mins).

Direction	U_H(m/s)	Response STD, σ		Crossing rate, ν_0		Kurtosis		Extreme, non-Gaussian		Mean extreme, non-Gaussian		Extreme sample	
		mean	CV	mean	CV	mean	CV	mean	CV	mean	CV	mean	CV
Alongwind	40	0.088	0.160	0.140	0.051	2.823	0.107	0.280	0.095	0.270	0.128	0.275	0.153
	60	0.256	0.159	0.149	0.035	2.779	0.114	0.805	0.090	0.782	0.156	0.792	0.152
	80	0.509	0.148	0.150	0.033	2.824	0.115	1.628	0.094	1.563	0.147	1.649	0.168
Crosswind	40	0.158	0.166	0.165	0.015	2.734	0.133	0.493	0.086	0.475	0.173	0.477	0.160
	60	0.633	0.143	0.170	0.006	2.580	0.123	1.869	0.076	1.841	0.122	1.762	0.115
	80	0.995	0.074	0.172	0.006	2.177	0.083	2.499	0.057	2.507	0.040	2.396	0.054

acceleration.

The time histories of building top displacement and acceleration in both alongwind and crosswind directions at $U_H = 40$, 60 and 80 m/s are simulated using the reduced-order model, where the mean alongwind load is not included. 200 response history samples are computed at each wind speed with consideration of parameter uncertainties, which can give sufficiently accurate estimation of response statistics. To study the sampling uncertainty, two sample durations of $T = 10$ and 60 mins are considered as the mean wind speed is traditionally averaged in 10 or 60 mins. The response history with a duration of 3900 s is computed, and the first 300 s is removed to avoid the transient effect. From each response history sample, the response STD, crossing rate ratio at zero level, kurtosis, and absolute maximum response are computed. The response process has zero skewness.

Fig. 6 portrays the time histories of displacements, and the generalized restoring force and displacement relations at $U_H = 40$, 60 and 80 m/s. The corresponding linear elastic displacement is also shown for comparison. It is evident that both alongiwind and crosswind responses at $U_H = 40$m/s and alongwind response at $U_H = 60$ m/s are elastic. The crosswind response at $U_H = 60$m/s shows slight inelasticity. The yielding level gets higher at $U_H = 80$m/s, where crosswind displacement shows more inelasticity than the alongwind displacement. The inelastic response is lower than the elastic response due to additional hysteretic damping caused by yielding. For instance, at $U_H = 80$m/s, the STDs of alongwind and crosswind displacements are reduced by 9.5% and 33.7% from the elastic responses respectively. The reductions in accelerations are 14.1% and 34.2%, respectively. The yielding causes low-frequency drift of alongwind displacement, which can be clearly observed in the alongwind restoring force and displacement relation.

Tables 2 and 3 list the mean and CV of these response statistics for $T = 10$ mins and 60 mins. The results without consideration of parameter uncertainties are listed in Tables 4 and 5. Tables 6 and 7 are the results for the acceleration with $T = 10$ mins. The CVs of STD of displacement and acceleration are also displayed in Figs. 7 and 8. It is observed that the mean of response STD calculated from these calculations can be considered identical. The STD of acceleration has almost same level of uncertainty as the STD of displacement. On the other hand, as shown by the alongwind response at $U_H = 40$m/s, the uncertainty of

Table 5
Mean and CV of statistics of displacements without parameter uncertainty ($T = 60$mins).

Direction	U_H(m/s)	Response STD, σ		Crossing rate, ν_0		Kurtosis		Extreme, non-Gaussian		Mean extreme, non-Gaussian		Extreme sample	
		mean	CV	mean	CV	mean	CV	mean	CV	mean	CV	mean	CV
Alongwind	40	0.089	0.035	0.141	0.014	2.976	0.060	0.341	0.081	0.326	0.052	0.333	0.092
	60	0.262	0.044	0.151	0.009	2.984	0.074	1.010	0.081	0.951	0.066	0.970	0.090
	80	0.524	0.041	0.148	0.019	3.012	0.068	2.021	0.082	1.913	0.064	1.996	0.099
Crosswind	40	0.159	0.042	0.166	0.004	2.959	0.082	0.609	0.078	0.575	0.069	0.577	0.100
	60	0.647	0.036	0.170	0.001	2.680	0.055	2.202	0.060	2.209	0.053	2.023	0.042
	80	0.993	0.023	0.172	0.002	2.190	0.032	2.697	0.042	2.706	0.016	2.562	0.045

Table 6
Mean and CV of statistics of accelerations with parameter uncertainty (T = 10mins).

Direction	U_H(m/s)	Response STD, σ		Crossing rate, ν_0		Kurtosis		Extreme, non-Gaussian		Mean extreme, non-Gaussian		Extreme sample	
		mean	CV	mean	CV	mean	CV	mean	CV	mean	CV	mean	CV
Alongwind	40	0.085	0.344	0.168	0.072	2.606	0.181	0.254	0.077	0.240	0.313	0.232	0.294
	60	0.263	0.318	0.169	0.083	2.711	0.158	0.814	0.084	0.770	0.295	0.737	0.278
	80	0.502	0.247	0.171	0.070	2.746	0.157	1.577	0.086	1.487	0.244	1.445	0.231
Crosswind	40	0.192	0.372	0.176	0.077	2.615	0.163	0.576	0.077	0.549	0.320	0.525	0.297
	60	0.736	0.229	0.175	0.069	2.496	0.135	2.105	0.071	2.061	0.186	1.919	0.165
	80	1.146	0.132	0.180	0.048	2.159	0.105	2.865	0.055	2.865	0.092	2.620	0.092

Table 7
Mean and CV of statistics of accelerations without parameter uncertainty (T = 10mins).

Direction	U_H(m/s)	Response STD, σ		Crossing rate, ν_0		Kurtosis		Extreme, non-Gaussian		Mean extreme, non-Gaussian		Extreme sample	
		mean	CV	mean	CV	mean	CV	mean	CV	mean	CV	mean	CV
Alongwind	40	0.079	0.165	0.167	0.067	2.696	0.165	0.245	0.083	0.232	0.186	0.226	0.177
	60	0.247	0.191	0.168	0.067	2.682	0.158	0.758	0.082	0.727	0.201	0.698	0.183
	80	0.495	0.174	0.172	0.063	2.770	0.159	1.571	0.088	1.483	0.178	1.443	0.176
Crosswind	40	0.176	0.184	0.177	0.063	2.677	0.162	0.541	0.081	0.520	0.198	0.504	0.179
	60	0.732	0.147	0.176	0.061	2.541	0.127	2.132	0.073	2.101	0.123	1.957	0.106
	80	1.171	0.072	0.181	0.035	2.131	0.085	2.894	0.054	2.903	0.037	2.662	0.040

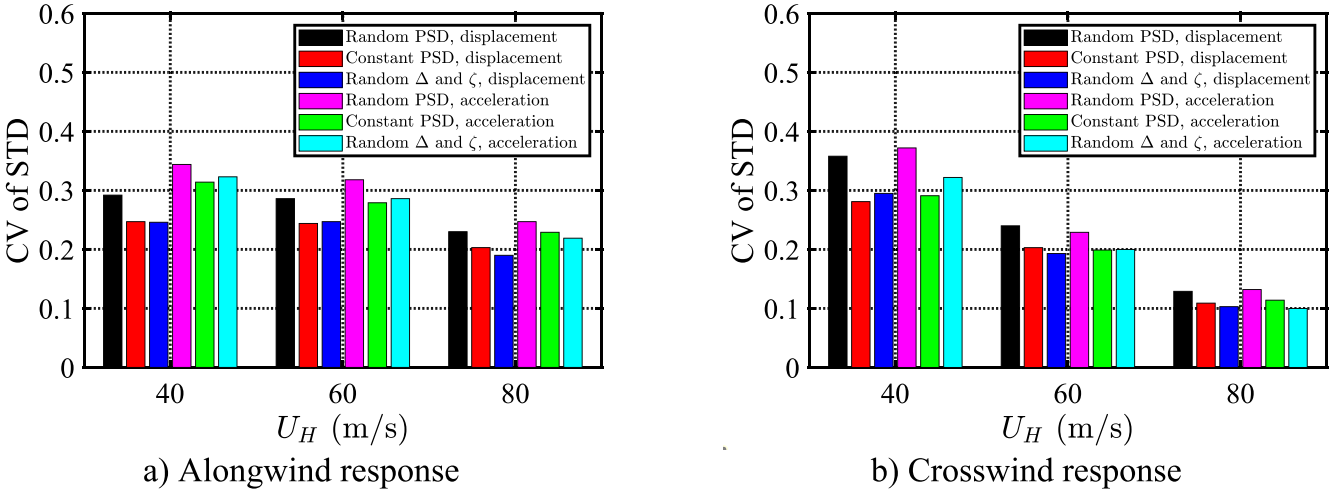

Fig. 7. CVs of STDs of building top displacements and accelerations (T = 10 mins).

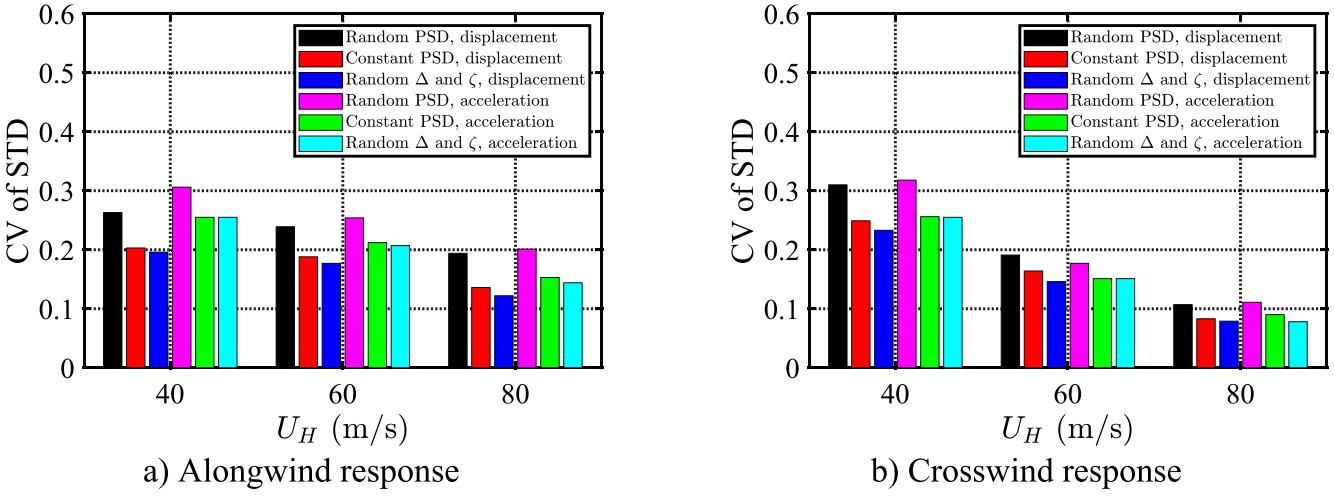

Fig. 8. CVs of STDs of building top displacements and accelerations (T = 60 mins).

Table 8
CV of STD and extreme value of displacements from various uncertainties.

Uncertainty		Randomness		Sampling uncertainty				Parameter uncertainty			
Response		Extreme		STD		Extreme		STD		Extreme	
Sample duration T(mins)		10	60	10	60	10	60	10	60	10	60
Alongwind	40 m/s	0.095	0.081	0.122	0.035	0.121	0.043	0.265	0.260	0.215	0.229
	60 m/s	0.090	0.081	0.159	0.044	0.122	0.039	0.237	0.235	0.208	0.237
	80 m/s	0.094	0.082	0.148	0.041	0.139	0.056	0.176	0.189	0.159	0.170
Crosswind	40 m/s	0.086	0.078	0.166	0.042	0.135	0.063	0.317	0.307	0.238	0.266
	60 m/s	0.076	0.060	0.143	0.036	0.086	0.000	0.193	0.187	0.152	0.121
	80 m/s	0.057	0.042	0.074	0.023	0.000	0.015	0.106	0.105	0.086	0.082

Table 9
CV of STD and extreme value of accelerations from various uncertainties.

Uncertainty		Randomness		Sampling uncertainty				Parameter uncertainty			
Response		Extreme		STD		Extreme		STD		Extreme	
Sample duration T(mins)		10	60	10	60	10	60	10	60	10	60
Alongwind	40 m/s	0.083	0.077	0.165	0.048	0.157	0.071	0.302	0.302	0.234	0.269
	60 m/s	0.082	0.080	0.191	0.052	0.164	0.066	0.254	0.248	0.210	0.234
	80 m/s	0.088	0.079	0.174	0.044	0.152	0.028	0.176	0.196	0.150	0.151
Crosswind	40 m/s	0.081	0.077	0.184	0.047	0.160	0.074	0.324	0.314	0.237	0.269
	60 m/s	0.073	0.058	0.147	0.037	0.077	0.000	0.176	0.173	0.126	0.097
	80 m/s	0.054	0.041	0.072	0.022	0.000	0.000	0.111	0.109	0.082	0.081

STD of displacement is slightly lower than the acceleration displacement which is attributed to the contribution of low-frequency background component that has lower uncertainty. The STD ratio of low-frequency to resonant alongwind displacement is 0.53 at $U_H = 40$m/s. The CVs of STDs calculated by response simulation with duration of $T = 60$mins are very close to those from the theoretical estimation in the case of elastic response. The uncertainty of elastic response STD is mainly influenced by uncertainty of modal damping ratio. The response with higher level of yielding has less uncertainty in its STD. It is because that the additional hysteretic damping has lower uncertainty, which leads to reduction of the uncertainty of total system damping. The uncertainty of inelastic response STD is primarily influenced by uncertainty of modal damping ratio and hysteretic damping. The simulation results with consideration of only uncertain parameters ϵ_Δ and ϵ_ζ (Figs. 7 and 8) demonstrated their dominant influence. The uncertainty of loading spectra increases the response uncertainty, but its influence reduces as the yielding level increases as shown in Figs. 7 and 8.

Two sources of uncertainty contribute to the CV of response STD, i.e., parameter uncertainty from structural model and wind loading spectra, and sampling uncertainty associated with simulation and use of limited length of response history for estimation. For instance of crosswind displacement at $U_H = 60$ m/s with duration of 10 mins, the CV of displacement STD with parameter uncertainty and sampling uncertainty is 0.240 (Table 2). It is 0.203 without the uncertainty of loading spectra (Fig. 7b). The CV is 0.143 without uncertainty of all parameters (Table 4), which is caused by sampling uncertainty. Clearly, the CV caused by all parameter uncertainty is calculated as $\sqrt{0.240^2 - 0.143^2} = 0.193$. The CV caused by uncertainty of loading spectra is $\sqrt{0.240^2 - 0.203^2} = 0.128$. Similar calculation can be made for the case with duration of 60 mins. The CVs caused by sampling uncertainty, parameter uncertainty and uncertainty of loading spectra are 0.036, 0.187 and 0.098. Tables 8 and 9 summarize the influence of various uncertainties on STDs of displacement and acceleration. As expected, the sampling uncertainty is reduced when longer duration of response is used for estimation. The influence of parameter uncertainty is not affected by the sample duration. The influence of parameter uncertainty is greater than the influence of sampling uncertainty.

4.2. Extreme response

The influence of uncertainty on the probability distributions of maximum alongwind and crosswind displacements and accelerations are also investigated. The mean and CV as well as the cumulative distribution functions (CDFs) of the extreme responses are directly calculated from 200 extreme response samples. The results are listed in Tables 2-7 in the column "Extreme sample". It is evident that the parameter uncertainty leads to a larger CV while has negligible influence on the mean of extreme. The CV of crosswind displacement at $U_H =$ 60 and 80 m/s is much lower, which is associated with hardening non-Gaussian distribution of the response with kurtosis less than 3 caused by significant level of yielding.

The CDF of extreme response is also calculated by using the upcrossing rate theory based on the mean of response statistics [43]. The CDF of extreme value of a Gaussian random process $R(t)$ within a time duration T, i.e., $R_{\max} = \max(|R(t)|)$, is calculated as follows based on Poisson assumption:

$$F_{\max}(r) = \exp\left[-2\nu_0 T \exp\left(-r^2/2\sigma_R^2\right)\right] \tag{17}$$

where $\nu_0 = \sigma_{\dot{R}}/(2\pi\sigma_R)$ is the mean upcrossing rate at zero mean.

For a non-Gaussian process $R(t)$, a monotonic translation model can be developed to relate it to an underlying standard Gaussian process $U(t)$, i.e., $R(t)/\sigma_R = g(U)$, where $g(\bullet)$ is translation function that can be established using CDF mapping or first four statistical moments (e.g., [13,14]). In this study, the response skewness is zero thus the translation model is determined by the response kurtosis. Accordingly, the CDF of extreme of non-Gaussian response is calculated as:

$$F_{\max}(r) \approx \exp\left[-2\nu_0 T \exp\left\{-\left[g^{-1}(r/\sigma_R)\right]^2/2\right\}\right] \tag{18}$$

where $g^{-1}(\bullet)$ is the inverse function of $g(\bullet)$. The mean and CV of the extreme are then computed using the probability density function of extreme. The mean extreme also corresponds to $F_{\max}(r) = 57\%$ when the extreme distribution is considered to follow the Gumbel (Type I) distribution.

Tables 2-7, column "Extreme, non-Gaussian", list the mean and CV of extreme calculated from crossing rate theory using means of the response statistics, i.e., STD, crosswind rate at zero mean and kurtosis.

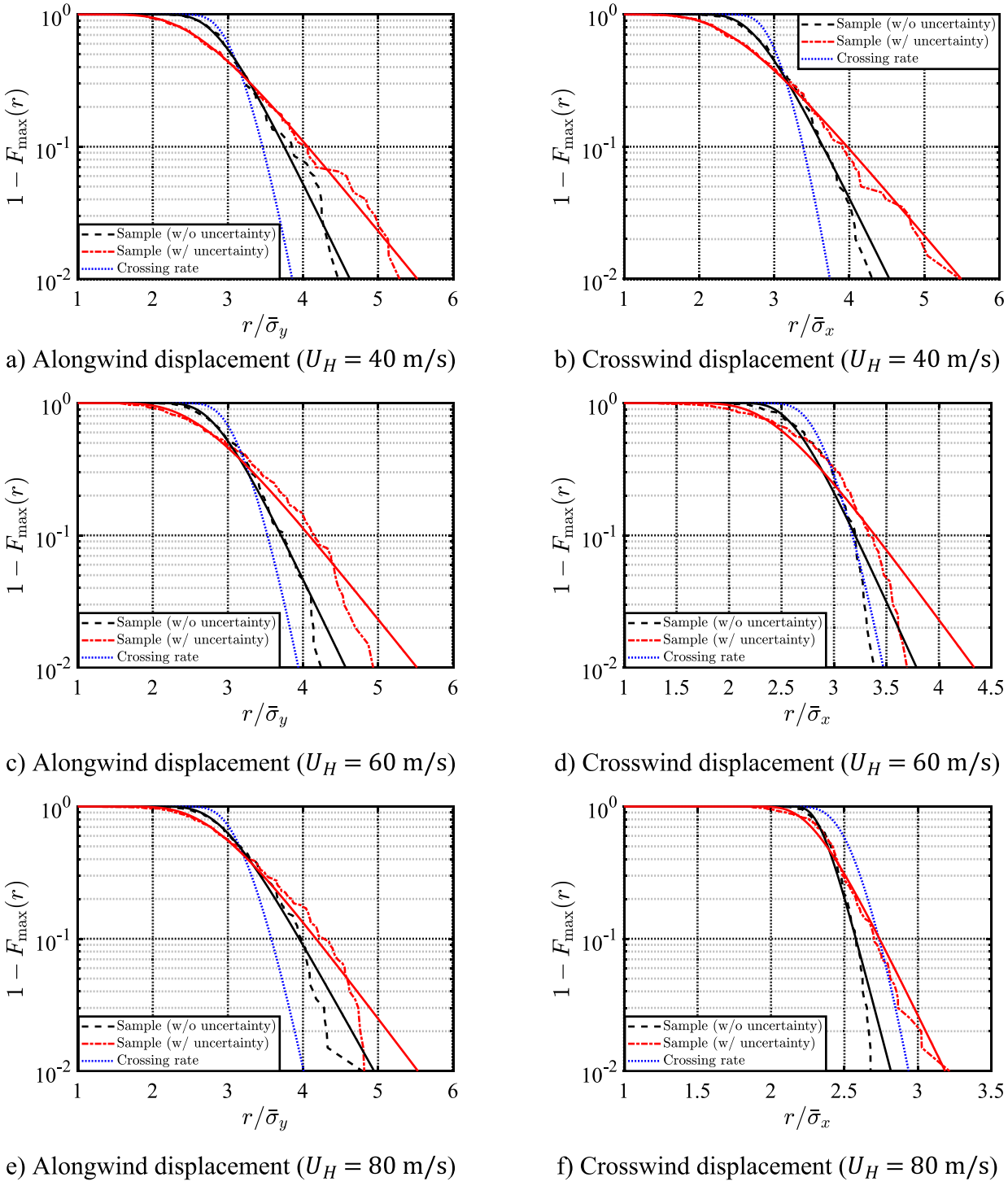

Fig. 9. CDFs of extreme displacements ($T = 10$mins).

This CV represents the influence of randomness on extreme. From the 200 sets of response statistics and by using the crossing rate theory, 200 estimations of mean extreme and extreme probability distributions are also calculated, from which the mean and CV of the estimated mean extreme are calculated and listed in the column "Mean extreme, non-Gaussian". It is noted that mean of extreme calculated from crossing rate theory is very close to that from extreme samples, which again illustrated the effectiveness of crossing rate theory and the kurtosis-based translation model.

Three sources of uncertainty contribute to the CV of extreme, i.e., randomness, parameter uncertainty and sampling uncertainty. The total CV can be given as square-root-of-sum-of-squares of these three CVs. The CV caused by randomness can be estimated from the extreme distribution determined using the crossing rate theory with means of the response statistics. The CV due to randomness calculated from response analysis with and without uncertainty can be considered identical. By comparing the CVs of extreme calculated with and without parameter uncertainty, the CV caused by parameter uncertainty can be determined. Subsequently, the CV caused by sampling uncertainty is then computed.

For instance of the crosswind extreme displacement with duration of $T = 10$ mins at $U_H = 60$ m/s, the CV caused by randomness is 0.076 according to column "Extreme, Non-Gaussian" in Table 4. The CVs with

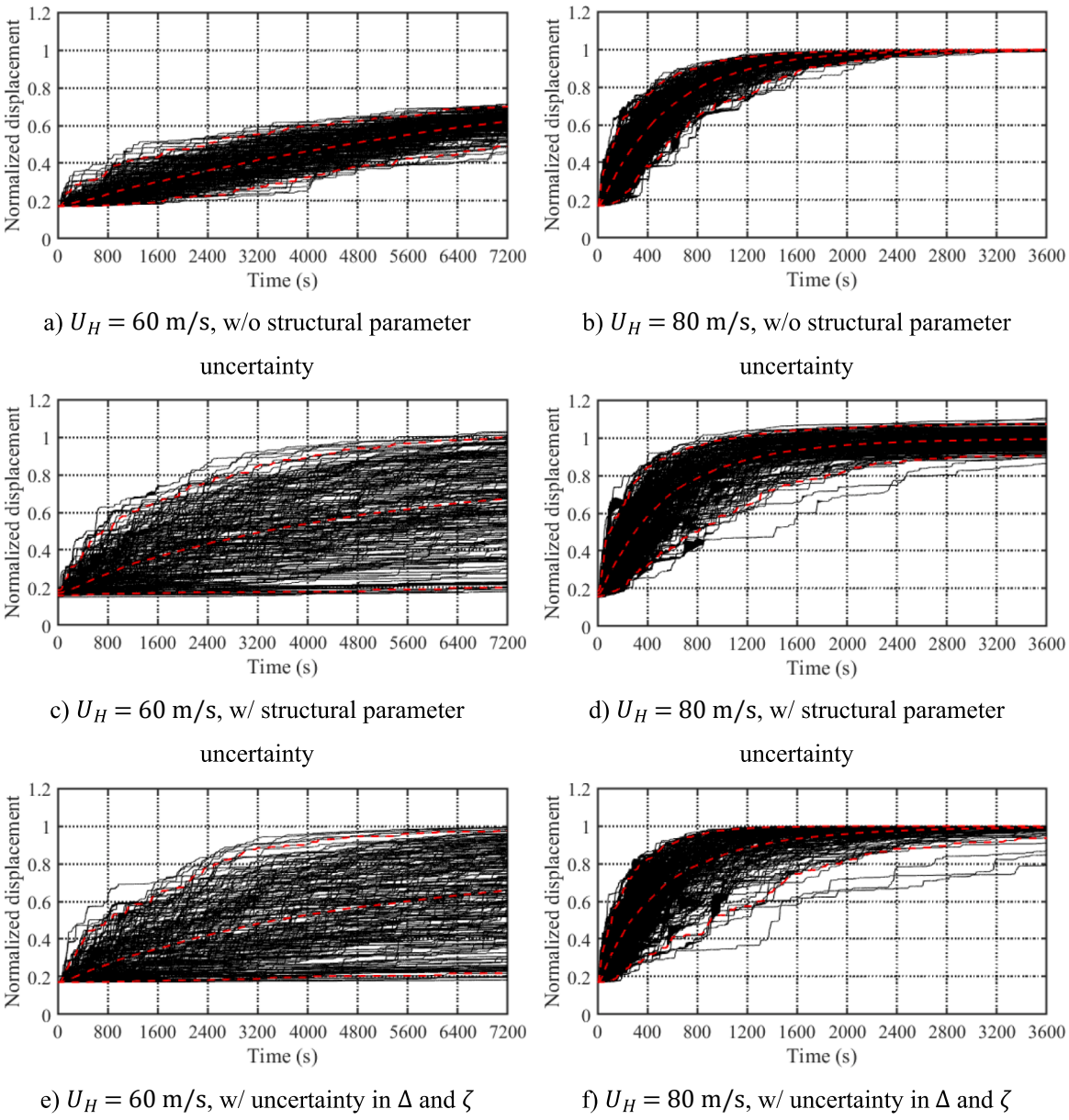

Fig. 10. Variation of time-varying mean alongwind displacements at building top.

and without parameter uncertainty are 0.190 and 0.115 according to Tables 2 and 4 directly estimated from extreme samples, i.e., the column "Extreme sample". Accordingly, the CV caused by sampling uncertainty is $\sqrt{0.115^2 - 0.076^2} = 0.086$. The CV caused by parameter uncertainty is calculated as $\sqrt{0.190^2 - 0.115^2} = 0.152$. On the other hand, for the case of $T = 60$ mins, the CV caused by randomness is 0.060 according to Table 5. The CVs with and without parameter uncertainty are 0.128 and 0.042 according to Tables 3 and 5. Thus, the CVs caused by sampling uncertainty and parameter uncertainty are 0.000 and 0.121. The reason that the CV without parameter uncertainty, i.e., caused by randomness and sampling uncertainty, is slightly less than the CV caused by randomness is attributed to numerical approximation especially that of crossing rate theory. The CV of extreme within a longer duration has less uncertainty while the mean of extreme increases. The CV of extreme crosswind response at $U_H = 60$ and 80 m/s is apparently lower, which is consistent to the observation of CV of response STD. The CV of extreme acceleration is very close to that of extreme displacement.

Tables 8 and 9 summarize the influence of various uncertainties on response STD and extreme. It is observed that the sampling uncertainty has almost same influence on the response STD and extreme, while less influence on extreme is observed for crosswind response at $U_H = 60$ and 80 m/s. The parameter uncertainty has less influence on response extreme as compared to response STD. Therefore, it will be conservative to use CV of response STD to approximate the CV of extreme response.

Fig. 9 displays the exceeding probability of extreme displacements, i.e., $1 - F_{\max}(r)$, respectively representing the distributions due to randomness, randomness plus sampling uncertainty, and further plus the parameter uncertainty. The extreme value distributions estimated from the samples (dashed or dotted lines) with and without parameter uncertainty are very close to Gumbel (Type I) distributions (continuous lines) determined from the mean and CV of extreme, which are shown in Fig. 9 along with the empirical distributions. Again, it is observed that the extreme crosswind responses at $U_H = 60$ and 80 m/s have less uncertainty.

4.3. Time-varying mean alongwind displacement

The alongwind inelastic displacement has time-varying mean

component when the static (mean) alongwind load is included in the analysis. The time-varying mean alongwind displacement at the building top at $U_H = 60$ and 80 m/s influenced by the uncertainties of structural parameters is investigated using the reduced-order building model, where the uncertainty of the wind loading spectral model is not included. A total of 200 response samples with time duration of 7200 s and time step of 0.04 s are generated. For the purpose of comparison, the response samples without consideration of uncertainty of structural parameters are also generated. Fig. 10 shows these samples normalized by the steady-state mean displacement, which is determined by the mean alongwind load and mean generalized second stiffness, i.e., $\mu_{Q_y}/\alpha_y K_{y0}$ [20,30]. Furthermore, the simulation with consideration of only uncertainty parameters ϵ_Δ and ϵ_ζ are also carried out, where the uncertainty in the building stiffness thus the uncertainty in the steady-state mean displacement is not included. Their ensemble means and 95% confidence intervals are also shown in Fig. 10. The lower and upper bounds of 95% confidence intervals correspond to 2.5% and 97.5% non-exceeding probabilities.

The ensemble means of the time-varying alongwind displacement calculated from three cases, i.e., Fig. 10a), c) and e), or Fig. 10b), d) and f), are almost identical. The time-varying mean alongwind displacement at $U_H = 80\text{m/s}$ approaches to steady-state value faster than that at $U_H = 60\text{m/s}$ due to higher level of yielding and more frequent drift. The uncertainty of time-varying mean displacement is attributed to randomness of dynamic response and the influence of parameter uncertainty. The CV of the steady-state mean displacement is 0.044, which is very close to the theoretical estimation, i.e., CV of $\mu_{Q_y}/\alpha_y K_y$ as 0.045, where the uncertainty of mean wind load is not considered in this study. The uncertainty in the transient state is larger than that of steady-state value. For example of response at $U_H = 60\text{m/s}$ and $t = 4800\text{s}$, the CV without structural parameter uncertainty, i.e., Fig. 10a), is 0.126. The CV with parameter uncertainty, i.e., Fig. 10c), is 0.378. The CV with uncertainties of dominant parameters but without uncertainty of steady-state mean is 0.371. Clearly, time-varying mean alongwind displacement is very sensitive to the parameter uncertainty especially the uncertainty in yielding displacement. It should be mentioned that although the time-varying mean response is overestimated by the reduced-order building model, the insights on the uncertainties of the time-varying mean response presented above remain valid.

5. Conclusions

The influences of various uncertainties in building model parameters and wind loading spectra on the predicted inelastic tall building displacements and accelerations were investigated using a 60-story steel building as an example. The results showed that the structural modal damping ratio and yielding displacement are two most influencing parameters contributing to uncertainty of response. With the increase in the level of yielding at higher wind speed, the influence of uncertainty of modal damping reduces, while the influence of uncertainty of yielding displacement becomes significant. The response with a higher level of yielding shows less uncertainty in its STD. The STD of acceleration has almost same level of uncertainty as the STD of displacement. The influence of parameter uncertainty is greater than that of sampling uncertainty.

Three sources of uncertainty contribute to the uncertainty of extreme, i.e., randomness, parameter uncertainty and sampling uncertainty. The uncertainty of extreme caused by randomness can be estimated from the extreme distribution using the crossing rate theory. The sampling uncertainty has almost same influence on the response STD and extreme. The parameter uncertainty has less influence on response extreme as compared to response STD. The response with a higher level of yielding shows hardening non-Gaussian distribution, which leads to less uncertainty of extreme response as compared to response STD. The distribution of extreme acceleration shows similar characters.

The uncertainty of time-varying mean alongwind displacement is influenced by the randomness of the fluctuation responses and the parameter uncertainty. The uncertainty of the transient phase of the time-varying mean displacement is larger than that of the steady-state mean value. The time-varying mean alongwind displacement is very sensitive to the parameter uncertainty, especially the uncertainty in yielding displacement. The uncertainty of state-state mean displacement is determined by the uncertainty of post-yielding stiffness and uncertainty of mean wind loading.

CRediT authorship contribution statement

Jinghui Huang: Formal analysis, Data curation, Software, Writing – original draft. **Xinzhong Chen:** Supervision, Methodology, Writing – review & editing.

Declaration of Competing Interest

The authors declare that they have no known competing financial interests or personal relationships that could have appeared to influence the work reported in this paper.

Data availability

Data will be made available on request.

Acknowledgment

The support for this work provided in part by National Science Foundation (NSF) grant No. CMMI-2153189 is greatly acknowledged.

References

[1] Architectural Institute of Japan (AIJ). AIJ recommendations for load on buildings. Tokyo: AIJ; 2004.
[2] ASCE, SEI. Prestandard for performance-based wind design. VA: Reston; 2019.
[3] Beck AT, Kougioumtzoglou IA, dos Santos KR. Optimal performance-based design of non-linear stochastic dynamical RC structures subject to stationary wind excitation. Eng Struct 2014;78:145–53.
[4] Bashor R, Kareem A. Load factors for dynamically sensitive structures. In: Proc., 11th Americas Conf. on Wind Eng. San: Juan, Puerto Rico; 2009.
[5] Chen X. Estimation of wind load effects with various mean recurrence intervals with a closed-form formulation. Int J Struct Stability Dynamics 2016;16:1550060-1.
[6] Chen X, Kareem A. Proper orthogonal decomposition-based modeling, analysis, and simulation of dynamic wind load effects on structures. J Eng Mech 2005;131(4):325–39.
[7] Chen X, Huang G. Estimation of probabilistic extreme wind load effects: Combination of aerodynamic and wind climate data. J Eng Mech 2010;136(6):1–14.
[8] Chuang WC, Spence SMJ. A performance-based design framework for the integrated collapse and non-collapse assessment of wind excited buildings. Eng Struct 2017;150:746–58.
[9] Chuang WC, Spence SMJ. An efficient framework for the inelastic performance assessment of structural systems subject to stochastic wind loads. Eng Struct 2019;179:92–105.
[10] Chuang WC, Spence SMJ. A framework for the efficient reliability assessment of inelastic wind excited structures at dynamic shakedown. J Wind Eng Ind Aerodyn 2022;220:104834.
[11] Cook NJ, Mayne JR. A novel working approach to the assessment of wind loads for equivalent static design. J Wind Eng Ind Aerodyn 1979;4:149–64.
[12] Cook NJ, Mayne JR. A novel working approach to the assessment of wind loads for equivalent static design a refined working approach to the assessment of wind loads for equivalent static design. J Wind Eng Ind Aerodyn 1981;8(3):299–301.
[13] Ding J, Gong K, Chen X. Comparison of statistical extrapolation methods for the evaluation of long-term extreme response of wind turbine. Eng Struct 2013;57:100–15.
[14] Ding J, Chen X. Assessment of methods for extreme value analysis of non-Gaussian wind effects with short-term time history samples. Eng Struct 2014;80:75–88.
[15] Ding J, Chen X. Fatigue damage evaluation of broad-band Gaussian and non-Gaussian wind load effects by a spectral method. Probab Eng Mech 2015;41:139–54.
[16] Diniz SMC, Simiu E. Probabilistic descriptions of wind effects and wind-load factors for database-assistant design. J Struct Eng 2005;131(3):2005.

[17] Diniz SMC, Sadek F, Simiu E. Wind speed estimation uncertainties: Effects of climatological and micrometeorological parameters. Probab Eng Mech 2004;19:361–71.
[18] Ellingwood BR, Tekie PB. Wind load statistics for performance-based structural design. J Struct Eng 1999;125(4):453–63.
[19] Feng C, Chen X. Crosswind responses of tall buildings with nonlinear aerodynamic damping and hysteretic restoring force character. J Wind Eng Ind Aerodyn 2017;167:62–74.
[20] Feng C, Chen X. Inelastic responses of wind-excited tall buildings: Improved estimation and understanding by statistical linearization approaches. Eng Struct 2018;159:141–54.
[21] Gani F, Légeron F. Relationship between specified ductility and strength demand reduction for single degree-of-freedom systems under extreme wind events. J Wind Eng Ind Aerodyn 2012;109:31–45.
[22] Ghaffary A, Moustafa MA. Performance-based assessment and structural response of 20-story sac building under wind hazards through collapse. J Struct Eng 2021;147(3):04020346.
[23] Griffis L, Patel V, Muthukumar S, Baldava S. A framework for performance-based wind engineering. In: Proc., Advances in hurricane engineering. Florida, USA: Miami; 2013. p. 1205–16.
[24] Hanzlik P, Diniz S, Grazini A, Grigoriu M, Simiu E. Building orientation and wind effects estimation. J Eng Mech 2005;131(3):254–8.
[25] Harris RI. An improved method for the prediction of extreme values of wind effects on simple buildings and structures. J Wind Eng Ind Aerodyn 1982;9:343–79.
[26] Harris RI. A new direct version of the Cook-Mayne method for wind pressure probabilities in temperate storms. J Wind Eng Ind Aerodyn 2005;93:581–600.
[27] Hart GC, Jain A. Nonlinear response of tall buildings subjected to wind loads. Struct Des Tall Spec Build 2011;20(S1):63–5.
[28] Hong HP. Accumulation of wind induced damage on bilinear SDOF systems. Wind Struct 2004;7(3):145–58.
[29] Huang JH, Chen X. Inelastic performance of high-rise buildings to simultaneous actions of alongwind and crosswind loads. J Struct Eng 2022;148(2):04021258.
[30] Huang JH, Chen X. Inelastic response of high-rise buildings under strong winds: Accuracy of reduced building model and influence of biaxial response interaction. J Struct Eng 2023;149(1):04022211.
[31] Judd JP, Charney FA. Inelastic behavior and collapse risk for buildings subjected to wind loads. In Structures Congress 2015:2483–96.
[32] Judd JP, Charney FA. Wind performance assessment of buildings. In: Proc., Geotechnical and Structural Engineering Congress; 2016. Reston, VA.
[33] Judd JP. "Windstorm resilience of a 10-story steel frame office building". ASCE-ASME J. Risk Uncertainty Eng. Syst., Part A. Civ Eng 2018;4(3):04018020.
[34] Liu M, Chen X, Yang Q. Estimation of multiple limit state responses with various mean recurrence intervals considering directionality effects. J Wind Eng Ind Aerodyn 2019;193:1–13.
[35] Lutes LD, Sarkani S. Random vibrations: analysis of structural and mechanical systems. Burlington, MA: Elsevier; 2004.
[36] McKenna F, Scott MH, Fenves GL. Nonlinear finite-element analysis software architecture using object composition. J Computing in Civil Eng 2010;24(1):95–107.
[37] Melchers RE, Beck AT. Structural reliability analysis and prediction. John Wiley & Sons; 2018.
[38] Mooneghi MA, Irwin P, Chowdhury AG. Exploratory studies on a bilinear aeroelastic model for tall buildings. In: Proc., 14th Int. Conf. Wind Eng. Brazil: Porto Alegre; 2015.
[39] NIST. Nonlinear structural analysis for seismic design: A guide for practicing engineers. NIST GCR 10-917-5. Gaithersburg, MD, 2010.
[40] Ohkuma T, Kurita T, Ninomiya, M. Response estimation based on energy balance for elasto-plastic vibration of tall building in across-wind direction. In Proc., 7th International Conference on Structural Safety and Reliability, Kyoto, Japan; 1997, p. 1379-86.
[41] Ouyang Z, Spence SM. Performance-based wind-induced structural and envelope damage assessment of engineered buildings through nonlinear dynamic analysis. J Wind Eng Ind Aerodyn 2021;208:104452.
[42] Park S, Yeo D. Second-order effect on wind-induced structural behavior of high-rise steel buildings. J Struct Eng 2018;144(2):04017209.
[43] Rice SO. Mathematical analysis of random noise. Bell Labs Tech J 1944;23(3):282–1232.
[44] Roberts JB, Spanos PD. Random vibration and statistical linearization. Courier Corporation; 2003.
[45] Shinozuka M, Jan CM. Digital simulation of random processes and its applications. J Sound Vib 1972;25(1):111–28.
[46] Spacone E, Filippou FC, Taucer FF. Fiber beam-column model for nonlinear analysis of R/C frames: part I. formulation. Earth Eng Struct Dyn 1996;25(7):711–25.
[47] Spence SMJ, Kareem A. Performance-based design and optimization of uncertain wind-excited dynamic building systems. Eng Struct 2014;78:133–44.
[48] Tabbuso P, Spence SM, Palizzolo L, Pirrotta A, Kareem A. An efficient framework for the elasto-plastic reliability assessment of uncertain wind excited systems. Struct Saf 2016;58:69–78.
[49] Tamura Y, Yasui H, Marukawa H. Non-elastic responses of tall steel buildings subjected to across-wind forces. Wind Struct 2001;4(2):147–62.
[50] Tian J, Chen X. Evaluation of wind directionality on wind load effects and assessment of system reliability of wind-excited structures. J Wind Eng Ind Aerodyn 2020;199:104133.
[51] Tsujita O, Hayabe Y, Ohkuma T. A study on wind-induced response for inelastic structure. In: Proc., ICOSSAR; 1997. p. 1359–66.
[52] Wang CH, Wen YK. Evaluation of pre-Northridge low-rise steel buildings. I: Modeling. J Struct Eng 2000;126(10):1160–8.
[53] Wu D, Chen X, Yang QS. Estimation of wind-induced extreme responses with various mean recurrence intervals considering model uncertainty due to limited data. J Wind Eng Ind Aerodyn 2016;158:81–97.
[54] Zheng XW, Li HN, Gardoni P. Reliability-based design approach for high-rise buildings subject to earthquakes and strong winds. Eng Struct 2021;244:112771.